Dyes and Pigments 205 (2022) 110557

Contents lists available at ScienceDirect

Dyes and Pigments

journal homepage: www.elsevier.com/locate/dyepig

# Synthesis of water-soluble hemicoronenediimides by photocyclization of perylenediimides: Turn-on fluorescent probes in water by complexation with Cucurbit[7]uril or binding to G-quadruplex Motifs

Natalia Busto [a,b,**], Daisy C. Romero [a], Andrea Revilla-Cuesta [a], Irene Abajo [a], José Vicente Cuevas [a], Teresa Rodríguez [a], Begoña García [a], Tomás Torroba [a,*]

[a] Departamento de Química, Facultad de Ciencias, Universidad de Burgos, Plaza Misael Bañuelos s/n, 09001, Burgos, Spain
[b] Departamento de Ciencias de la Salud. Facultad de Ciencias de la Salud, Universidad de Burgos, Paseo de los Comendadores, s/n, 09001, Burgos, Spain

ARTICLE INFO

*Keywords:*
Perylenediimides
Hemicoronenediimides
Photocyclization
Nanoparticles
G-quadruplex
Cucurbituril
Cytotoxicity

ABSTRACT

A new series of perylene and hemicoronene diimides, obtained by visible light photocyclization, are presented, between them some remarkable examples that are soluble in only water, and give nanoparticles by self-association. Those compounds work as new fluorescent materials in water by complexation with cucurbit[7]uril, as well as selective G-quadruplex binding ligands with remarkable cytotoxic activity when the interaction with G4 was sufficiently strong.

## 1. Introduction

Fluorescent organic nanoparticles constitute an active subject of research in pharmacological transport or sensing devices as an alternative to the noble metal classic nanoparticles [1,2]. Assembling of organic nanoaggregates has been a rich source of nanomaterials for practical applications [3–6]. The study of aggregation of perylenediimides [7] has established an archetype in organic nanoaggregation [8–13]. Water-soluble perylenediimides and their self-organized nano--architectures had enormous implications in biology and materials [14–20]. Extended hemicoronenediimides have been intensely studied as well, on the way to valuable semiconducting materials [21–27] We have previously reported the ability of a water-soluble perylenediimide to bind to G-quadruplex structures in solution and its application as a new molecular tool for fishing these G-quadruplexes in solution [28] Some previous studies have found good binding activity to some water-soluble coronene [29–31] and hemicoronene [32] derivatives. Fluorescent sensing of G-quadruplex structures constitutes a powerful way to elucidate their biological role [33,34] and discrimination between G-quadruplex over duplex is a challenging but crucial goal in cellular studies [35] Despite the recent advances made in the development of selective fluorescent probes for G-quadruplex structures [36,37], new G-quadruplex lighting-up probes are valuable tools for cellular imaging. We have now designed an easy route to water soluble hemicoronenediimide derivatives having an aromatic core, encircled by a hydrophilic periphery, that are suitable for self-assembly applications and new fluorescent nanomaterials. We have also extended the synthesis to their corresponding hydrophobic counterparts, showing that the hydrophilicity is important for their exceptional characteristics. In this paper we want to introduce their synthesis, their notable self-assembly characteristics, their unique applications as supramolecular turn-on fluorescent materials in water, and their emission upon binding to G-quadruplex structures.

## 2. Results and discussion

Our synthesis started by the Suzuki reaction of the bromoperylenediimide **1** with one equivalent of a *N*-Boc protected piperazinyl-pyrimidine boronic ester **2** (Scheme 1) in conditions previously established by the group for related Suzuki reactions [38–40] The *N*-Boc protected derivative **3** (90% yield) was obtained after work-up of the reaction. Irradiation of **3** in dichloromethane (DCM) under visible light

* Corresponding author.
** Corresponding author. Departamento de Química, Facultad de Ciencias, Universidad de Burgos, Plaza Misael Bañuelos s/n, 09001, Burgos, Spain.
*E-mail addresses:* nbusto@ubu.es (N. Busto), ttorroba@ubu.es (T. Torroba).

https://doi.org/10.1016/j.dyepig.2022.110557
Received 28 April 2022; Received in revised form 2 July 2022; Accepted 4 July 2022
Available online 19 July 2022

(halogen lamp, 50W, 4 cm distance) and open air for 3 h, gave **4** (95% yield). Finally, *N*-Boc deprotection of all compounds by treatment with trifluoroacetic acid in DCM for 20 min quantitatively gave the unprotected compounds **5** and **6**, both of them bearing three unprotected secondary amine groups on the periphery (Scheme 1).

After collecting the physicochemical characteristics of the obtained compounds, we noted that the *N*-Boc protected compounds **3** and **4** were somewhat fluorescent in solutions of a few organic solvents, showing low quantum yields, from 0.3 to 0.6 in DCM or $CHCl_3$, and typical lifetimes of 5 ns (see Experimental section for details). Instead, the unprotected compounds **5** and **6**, were almost non-fluorescent compounds, soluble in water but almost non-soluble in common organic solvents.

Deposition of 2 μL of a recently prepared sample of **6** on a mica sheet showed, after evaporation of water, the presence of stable spherical nanoparticles in AFM (tapping mode, force constant 2.8 N $m^{-1}$, room temp., scan rate 1–2 lines per second). Instead, the non-cyclized relative of the latter compound, **5**, showed mainly the presence of microplates in AFM (Fig. 1).

The water-soluble nanoparticles from **5** and **6**, were also characterized by DLS (Figs. S26-S27 and S39-S41).

The study of aggregation or disaggregation related to fluorescence variations in low molecular weight organic nanoparticles in water constitutes an outstanding approach to new supramolecular systems; therefore, we tested the ways to mastering the disaggregation mechanism by molecular recognition.

### 2.1. Host-guest interactions with cucurbiturils

The piperidine and the piperazine groups on the boundaries of the obtained compounds are expected to interact easily with cucurbiturils in water [41,42]. Cucurbiturils have been used for the preparation of supramolecular luminescent sensors [43], light-harvesting materials [44], for enhancing fluorescence of perylenediimides in water [45,46] and several supramolecular applications [47–50]. To test the interactions, we performed experiments by adding aqueous solutions of cucurbit[n]urils: CB [5], CB [6], CB [7] and CB [8], in 1:1, 1:5, 1:10 and 1:20 colorant/cucurbituril molar proportions to 10 μM aqueous solutions of **5** or **6**. The compounds showed a neat increase of fluorescence in the presence of CB [7] exclusively (Fig. 2).

The fluorescent titration curves and the titration profiles of 10 μM solutions of **5** and **6** in water, with increasing amounts of CB [7], showed an asymptotic increase of fluorescence until a large excess of CB [7] was added (Fig. 2). In this way, **5** and **6** solutions in water became brightly fluorescent in the presence of a large excess of CB [7], constituting additional examples of the existing short collection of fluorescent perylene- and hemicoronenediimides in water solutions. CB [7] usually hosts smaller molecular guests [46,47,51,52] than the larger CB [8] which is able to host large aromatic hydrocarbons [41,44,45,53,54] Therefore, in this series the complexation with CB [7] should happen by the periphery of the compounds giving rise to disaggregation to form individual complexes in solution. Assuming this head to tail model, the achieved values for **5**@2CB [7] system were $K_1 = 883 \pm 26\ M^{-1}$ and $K_2 = 4190 \pm 370\ M^{-1}$ and for **6**@2CB [7], $K_1 = 219 \pm 63\ M^{-1}$ and $K_2 = 8989 \pm 728\ M^{-1}$ by using the Thordarson models [55–57]. To understand the interactions, we performed theoretical DFT calculations of the expected complexes (Fig. 3) and further calculations of stability (see the Supporting Information, Table S02, pp. S33–S34). The structures of the species formed in the interaction of **5** and **6** with two molecules of CB [7] were modelled using DFT calculations (see Experimental section for details). Two possibilities were explored for each compound, the interaction of the two CB [7] units through the apical piperidine groups or the interaction of one CB [7] through the apical piperidine group and the second CB [7] surrounding the equatorial piperazine ring. For **5**, the option with both units CB [7] located through the apical piperidine heterocycles is found to be 7.34 kcal/mol less stable than the option with one CB [7] unit surrounding one apical piperidine ring and the second

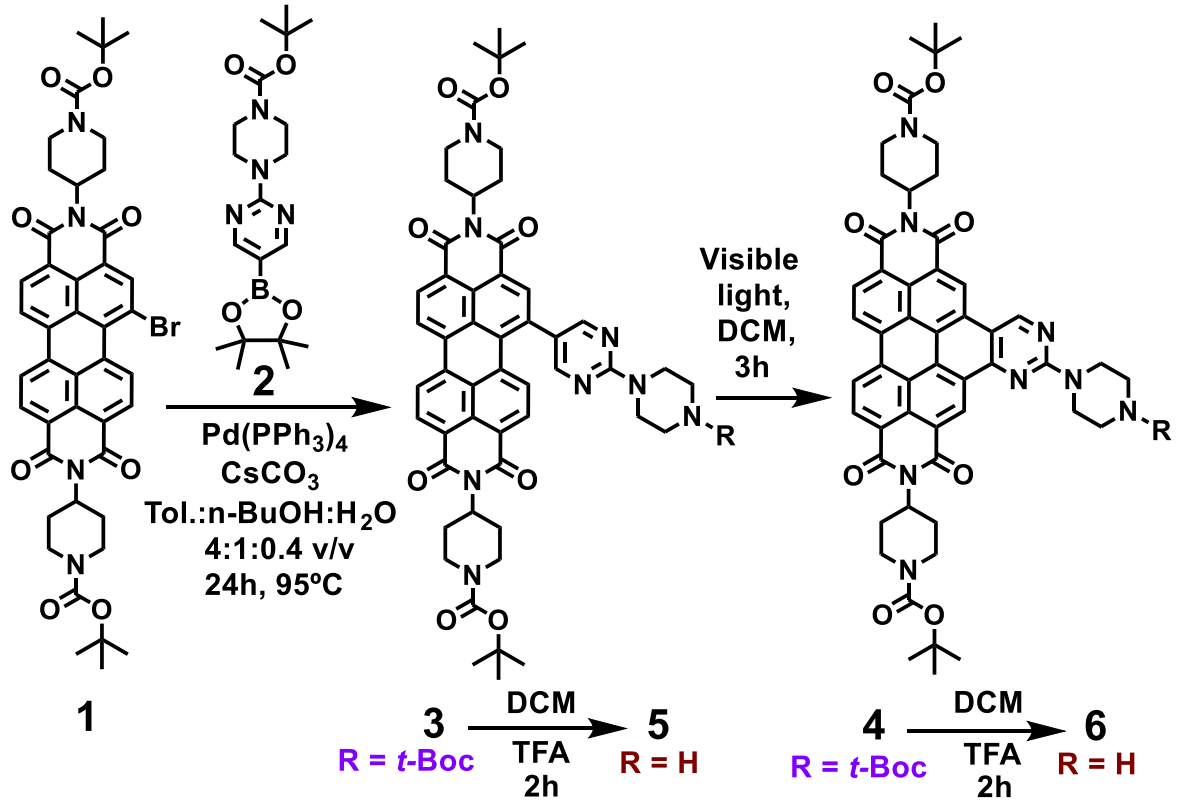


**Scheme 1.** Synthesis of perylene- and hemicoronenediimides.

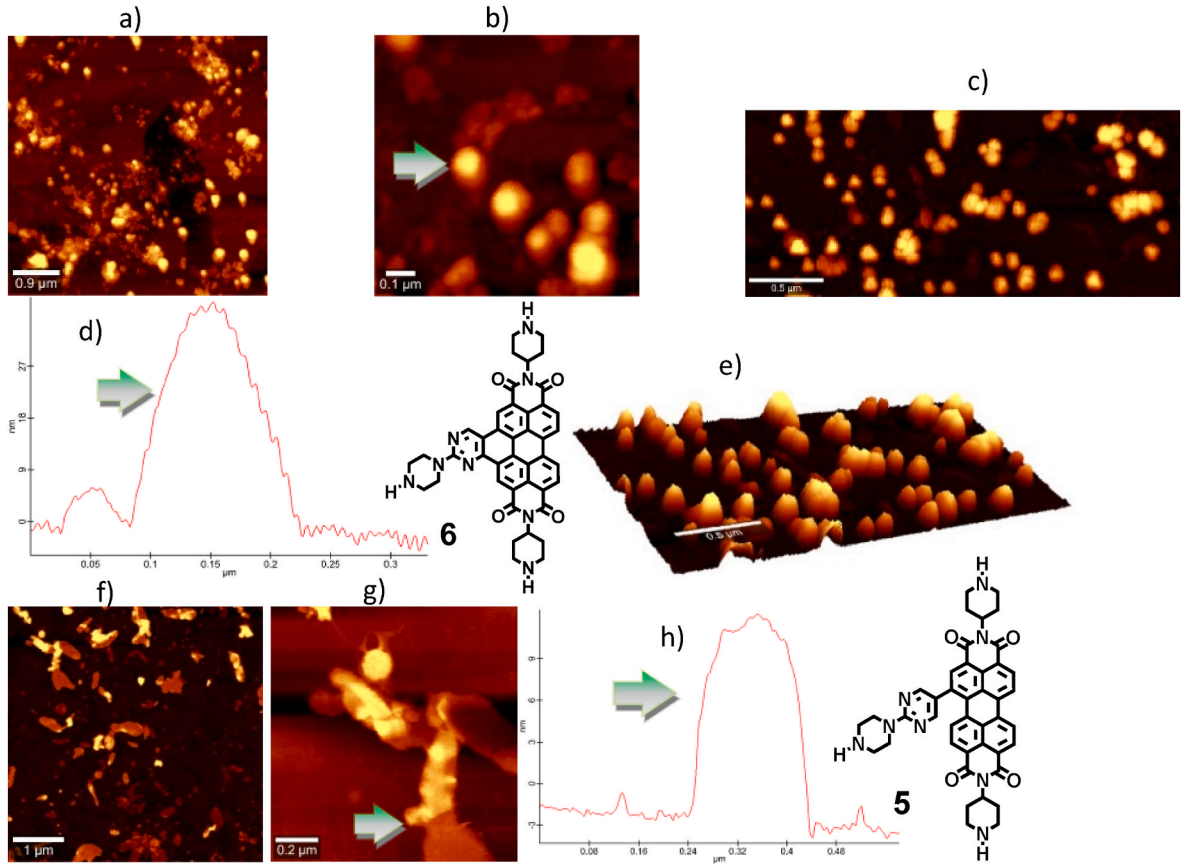


**Fig. 1.** AFM images of samples deposited on mica sheets from water solutions 0.1 μg/mL: (a)(b)(c) samples of **6** at different scales, (d) outline of a typical spherical nanoparticle of **6**, (e) 3D view of a sample of **6**. (f)(g) AFM images of samples of **5** at two scales, (h) outline of a typical nanoplate of **5**.

CB [7] unit surrounding the equatorial piperazine ring. Interestingly, for **6** the option that locates both CB [7] units surrounding the apical piperidine groups is found to be 11.10 kcal/mol more stable than the option in which there is one CB [7] unit surrounding one apical piperidine ring and the second CB [7] unit is surrounding the equatorial piperazine ring, exhibiting the enhanced rigidity of the hemicoronene core system (Fig. 3).

The theoretical calculations supported that $K_{1:1}$ should be greater than $K_{1:2}$ but, according to the Thordason model, for 5@2CB [7] system, $K_1$ is much lower than $K_2$ and for 6@2CB [7], $K_1$ is also much lower than $K_2$ which is not expected; but we should take into account that disaggregation equilibria are at work because these compounds formed high order aggregates (Fig. 1 and Supp. Info. S26–S27 and S39–S41). Thus, our experimental $K_1$ is a pseudo-constant that includes the disaggregation constant ($K_D$) and the binding constant $K_{1:1}$. Since the analytical concentration used for the calculation of the binding constants is too high in relation to the available concentration of the monomer species, this binding constant $K_1$ is underestimated.

### 2.2. Interaction with G-quadruplex structures

In the initial tests, **5** and **6** were not sensitive to common cations, anions, acids or oxidants, but they could be applied to the detection of biomolecules in solution, concretely to the non-canonical highly polymorphic G-quadruplex structures (G4). We tested the ability of compounds **5** and **6** to "turn on" their emission upon G-quadruplex binding. We included three G-quadruplexes with different topologies (a parallel: c-myc, an antiparallel: CTA22 and a hybrid type, hTelo) and a duplex (ctDNA) to investigate their topological preference as well as their selectivity towards G-quadruplex over duplex DNA. Both probes were selective for G-quadruplex since no emission was detected upon duplex addition (Fig. 4). By contrast, they "turned on" their emission in the presence of G-quadruplex structures. **5** was the most sensitive probe, being its fluorescence highly enhanced upon the addition of equimolar amounts of the antiparallel G-quadruplex CTA22.

In order to confirm the G4 binding ability of the previously synthesized water-soluble compounds, **5** and **6**, FRET melting assays were performed. Several G4 oligonucleotides in different conformations, parallel (c-myc, 25Ceb, 21R), antiparallel (21CTA, TBA, Bom17) and hybrid-type (hTelo) quadruplexes as well as an intramolecular duplex (dX) were included. The radar plot of the ΔTm of various oligonucleotides in the presence of **5** and **6** is shown in Fig. 5. From these results we can see that perylenediimide **5** and the hemicoronene **6** showed very good thermal stabilization values under the experimental conditions, especially for **5**, with the highest stabilizing effect on antiparallel G4s over the parallel G4s. These results are in good agreement with fluorescence measurements.

To understand the interaction between **5** and CTA22 a molecular docking study was performed to predict the most stable conformations of the interaction in the simplest 1:1 complex. The lower energy structure from the docking study was then further optimized using the semiempirical GFN2-xTB method (See Experimental part) (Fig. 6).

The calculation structure showed a remarkable molecular complementarity between CTA22 and **5**, the lateral pyrimidine group in this case looked to play a crucial role in the molecular interaction, and the restricted rotation of the group possibly contributed to the increased fluorescence of the complex. The analysis of the interactions between **5** and CTA22 did not show π-stacking interactions between the base pairs and the perylene moiety (see the Supporting Information Figs. S66–S70). Instead, **5** and CTA22 were bonded through hydrogen bond interactions between hydrogen atoms of deoxyribose in adenine-7/guanine-9, or the $NH_2$ group of adenine-19, and oxygen atoms of

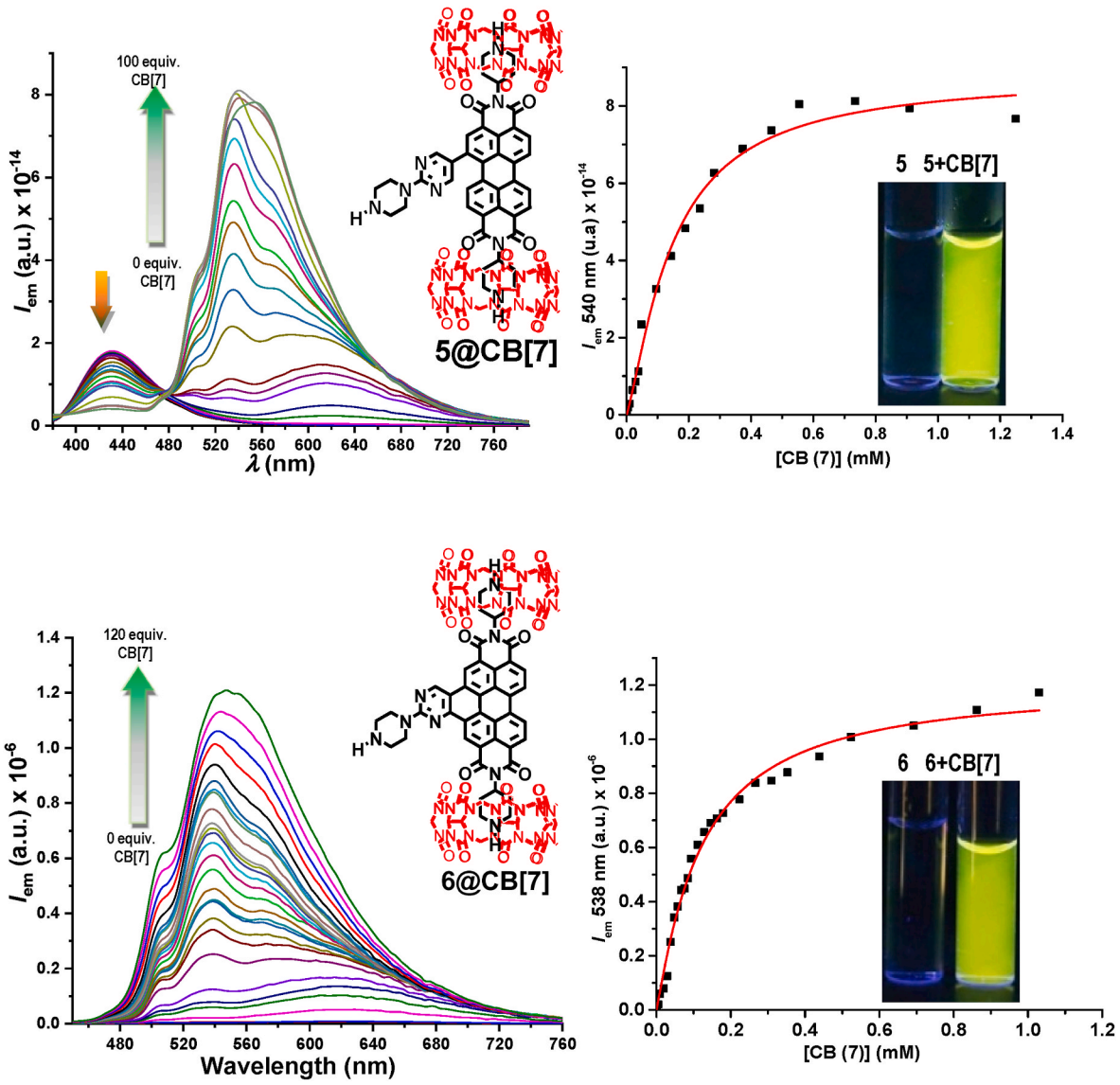


**Fig. 2.** Fluorescent titration curves and titration profiles of 10 μM solutions of **5** and **6** in water with increasing amounts of CB [7]. Inset: solution samples of **5** and **6** under UV light, 365 nm, before and after titrations with CB [7].

the diimide groups of **5**.

### 2.3. Cellular studies

To enable the potential application of these materials in biological media, it is important to evaluate their toxicity. **5** and **6** could be internalized and visualized in A549 (lung adenocarcinoma) cells after 1h of incubation (See the Supporting Information Figs. S71–S72). Then, their antiproliferative activity was tested by means of the MTT Assay. The biological behavior strongly differs since **6** is not cytotoxic in tumor A549 and non-tumor Hek293 cells after 72h of treatment. By contrast, **5** is a cytotoxic compound. In fact, apoptotic bodies were observed after 6h of treatment with 10 μM of **5** (Supp. Info. S73). The half maximal inhibitory concentration ($IC_{50}$ value) was calculated and compared with the widely applied anticancer agent cisplatin (CDDP). **5** (1.3 ± 0.1) is more cytotoxic than CDDP (4.0 ± 0.4) in lung adenocarcinoma cells (A549). Interestingly, the $IC_{50}$ value in A549 cells was lower than in non-cancer Hek239 cells (30.6 ± 1.5), revealing some selectivity of **5** towards cancer cells (Fig. 7). Therefore, a better performance in fluorescence increase in the presence of G4 and cytotoxic activity was found for the perylenediimide **5** than for the hemicoronene **6**.

## 3. Experimental

**General procedure for the Suzuki coupling.** *N,N′*-Bis-(1-(*tert*-butoxycarbonyl)piperidin-4-yl)-1-bromoperylene-3,4:9,10-tetracarboxylic diimide (1) (230 mg, 0.28 mmol) was dissolved in toluene:*n*-butanol:water (4:1:0.4) (65 mL) in a dried Schlenk flask under an inert atmosphere. Then, $Pd(PPh_3)_4$ (31.2 mg, 0.03 mmol), cesium carbonate (140 mg, 0.41 mmol) and 2-(4-(*N*-*tert*-butyl-1-carboxylate)piperazin-1-yl)pyrimidine-5-boronic acid pinacol ester 2 (110 mg, 0.28 mmol) were added. The reaction mixture was stirred under reflux (95 °C) for 24 h. A color change of the reaction mixture from red to dark red was observed. The solvent was removed under reduced pressure and the residue was subjected to column chromatography (silica gel, $CH_2Cl_2$:MeCN, 2:1 to $CH_2Cl_2$:MeOH, 50:1) to afford the monosubstituted perylenediimide 3 as a red solid (252 mg, 90%).

*N,N′*-Bis-(4-(*tert*-butoxycarbonyl)piperidin-4-yl)-1-((4-(*tert*-butoxycarbonyl)piperazin-1-yl)pyrimidin-1-yl)perylene-3,4:9,10-tetracarboxylic diimide 3. MP (°C): >350 °C. $R_f$ ($CH_2Cl_2$:MeOH, 50:2): 0.40. FT-IR (KBr, $cm^{-1}$): 3055 (C–H, aromatic), 2975 (C–H, aromatic), 2930 (C–H, aliphatic), 2860 (C–H, aliphatic), 1696 (C═O, carbamate), 1654 (C═O, imide), 1591, 1514 (C═C), 1480, 1424 (C–N), 1361 (C–N),

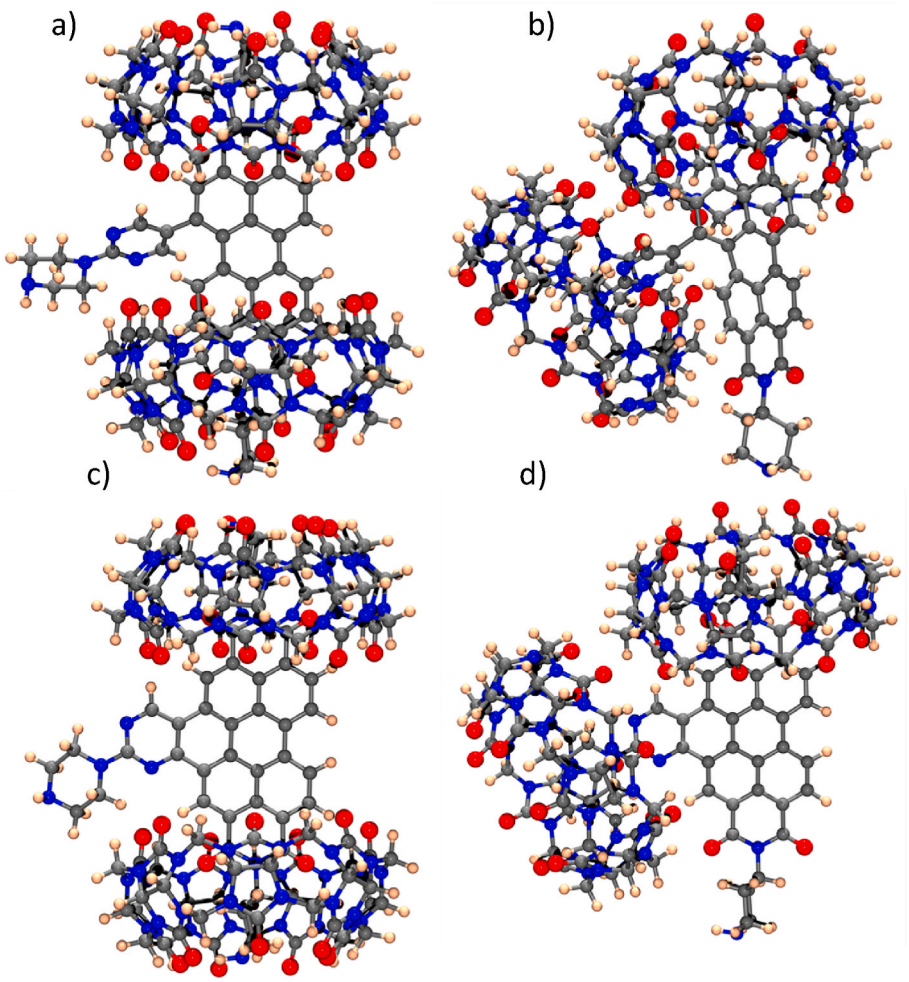


**Fig. 3.** (a) Calculated structure of complex **5**@2(*apical*)CB [7], relative energy (7.34 kcal/mol), and (b) **5**@2(*apical-equatorial*)CB [7], relative energy (0 kcal/mol). (c) Calculated structure of complex **6**@2(*apical*)CB [7], relative energy (0 kcal/mol), and (d) **6**@2(*apical-equatorial*)CB [7], relative energy (11.10 kcal/mol).

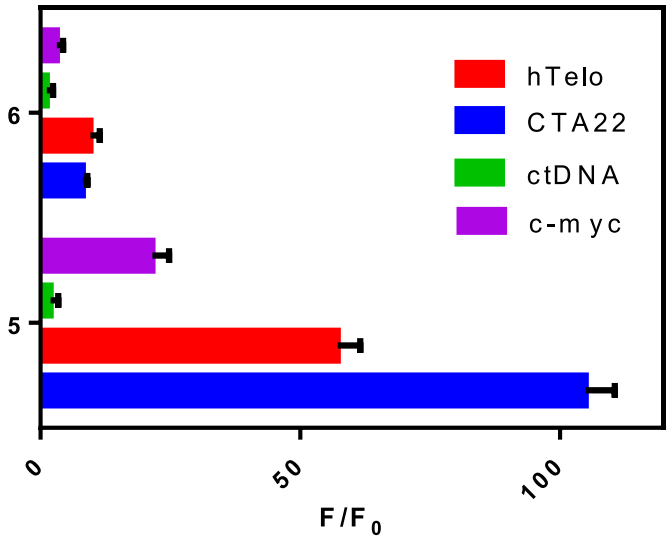


**Fig. 4.** Variation of the fluorescence intensity of 5 μM of **5** and **6** in the presence of 5 μM of hTelo, CTA22, c-myc and 10 $\mu M_{BP}$ ctDNA. [Probe]/[G4] = 1 and [Probe]/[duplex] = 0.5.

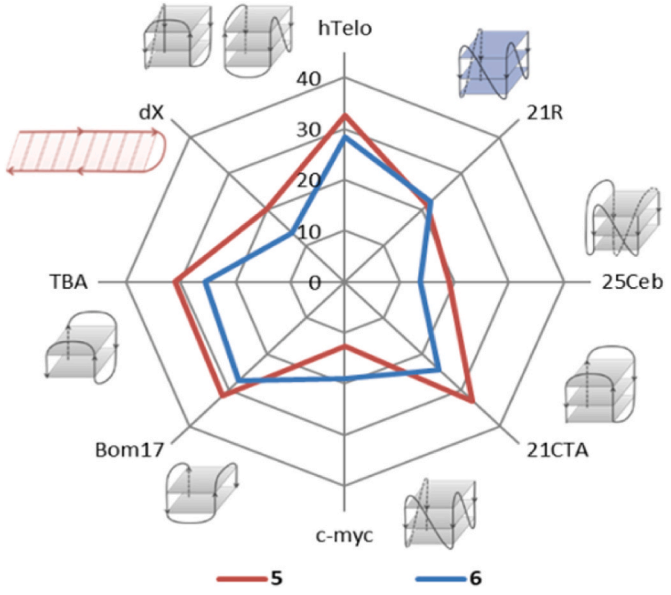


**Fig. 5.** Radar plot of the ΔTm of various oligonucleotides in the presence of 10 μM of **5** and **6**. All fluorescent oligonucleotides were tested at 0.2 μM strand concentration. [probe]/[oligo] = 50.

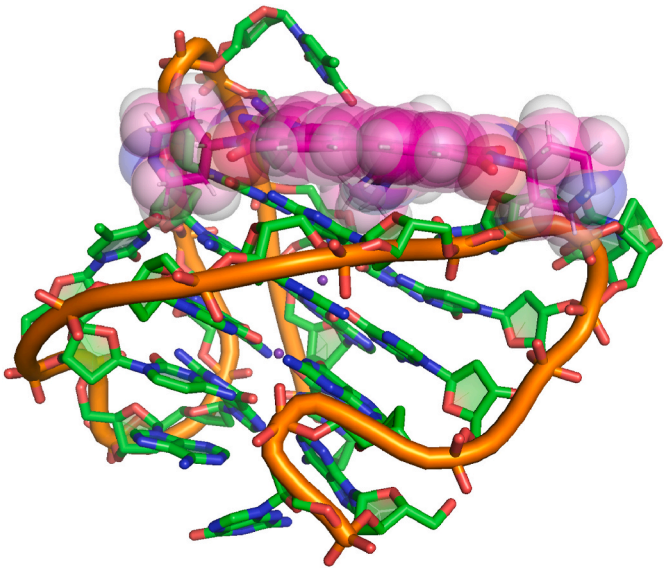

**Fig. 6.** Calculated structure of the complex between **5** and CTA22.

1341, 1274, 1246, 1170 (C–N), 1117, 1026, 992, 968, 943, 860, 808, 748, 720 (fingerprint region). $^{1}$H NMR (300 MHz, $CDCl_3$) $\delta$: 8.67 (d, $J$ = 8.1 Hz, 1H, Ar–H), 8.66 (d, $J$ = 8.1 Hz, 1H, Ar–H), 8.49 (s, 1H, Ar–H), 8.43 (s, 2H, 2 × Ar–H), 8.30 (d, $J$ = 8.3 Hz, 1H, Ar–H), 8.29 (d, $J$ = 8.1 Hz, 1H, Ar–H), 8.19 (d, $J$ = 8.3 Hz, 1H, Ar–H), 8.10 (d, $J$ = 8.1 Hz, 1H, Ar–H), 5.26–5.11 (m, 2H, N–CH), 4.44–4.22 (m, 4H, 2 × $CH_2$), 3.94–3.89 (m, 4H, 2 × $CH_2$), 3.61–3.56 (m, 4H, 2 × $CH_2$), 2.92–2.68 (m, 8H, 2 × $CH_2$), 1.74–1.66 (m, 4H, 2 × $CH_2$), 1.52 (s, 9H, 3 × $CH_3$), 1.51 (s, 9H, 3 × $CH_3$), 1.50 (s, 9H, 3 × $CH_3$). $^{13}$C NMR (75 MHz, $CDCl_3$) $\delta$: 163.9 (C═O), 163.7 (C═O), 163.6 (C═O), 160.9 (C═O),157.8 (C═O), 154.8 (C═O), 135.9 (CH), 135.7 (CAr), 134.9 (CAr), 134.9 (CAr), 134.5 (CAr), 133.4 (CH), 131.2 (CAr), 130.6 (CAr), 129.3 (CAr), 124.9 (CH), 124.0 (CAr), 123.7 (CAr), 123.5 (CAr), 123.2 (CAr), 123.0 (CAr), 122.9 (CAr),122.9 (CAr), 80.3 (C), 79.8 (C), 79.8 (C), 52.3 (CH), 52.2 (CH), 43.9 ($CH_2$), 29.8 ($CH_2$), 28.7 ($CH_3$), 28.6 ($CH_3$), 28.4 ($CH_2$). HR-MS (MALDI-, DIT): *m/z* calcd. for $C_{57}H_{62}N_8O_{10}$ ($[M]^-$): 1018.4583; found: 1018.4367. UV-VIS ($CH_2Cl_2$) $\lambda_{max}$/nm ($\varepsilon/M^{-1}\cdot cm^{-1}$): 540 (12971). Emission ($CH_2Cl_2$, $\lambda_{ex}$ = 437 nm) $\lambda_{max}$/nm: 632. $\tau$/ns ($CH_2Cl_2$, $\chi$2): 4.90, (1.12). $\Phi$ ($CH_2Cl_2$, $\lambda_{ex}$ = 455 nm): 0.34 ± 0.01.

**General procedure for the photochemical ring-closing reaction.** Substituted perylenediimide 3 (76 mg, 0.075 mmol) in $CH_2Cl_2$ (150 ml) was stirred under visible light irradiation (halogen lamp, GE M280/FNV/CG 50W 12 V, 50W, GU5.3 2900 K, General Electric) at 4 cm of distance for 3 h. The solvent was removed under reduced pressure and the residue was subjected to column chromatography (silica gel, $CH_2Cl_2$: MeCN, 5:1) to afford 4 (71 mg, 94% yield) as a purple solid.

*N*,*N*′-Bis-(1-(*tert*-butoxycarbonyl)piperidin-4-yl)-[6,7-e]-(2-(4-(*tert*-butoxycarbonyl)-1,4-piperazin-1-yl)-1,3-pyrimidin)perylene-3,4:9,10-tetracarboxylic diimide 4. MP (°C): >350 °C. $R_f$ ($CH_2Cl_2$:MeOH, 50: 2): 0.41. FT-IR (KBr, $cm^{-1}$): 2968 (C–H, aromatic), 2923 (C–H, aliphatic), 2857 (C–H, aliphatic), 1696 (C═O, carbamate), 1658 (C═O, imide), 1598, 1522 (C═C), 1434, 1417 (C–N), 1365 (C–N), 1320, 1250, 1170 (C–N), 1117, 1024, 814, 720 (fingerprint region). $^{1}$H NMR (300 MHz, $CHCl_3$) $\delta$: 9.45–8.89 (m, 3H, 3 × Ar–H), 8.66–8.42 (m, 4H, 4 × Ar–H), 5.36–5.19 (m, 2H, 2 × N–CH), 4.62–4.37 (m, 4H, 2 × $CH_2$), 4.15–3.99 (m, 4H, 2 × $CH_2$), 3.80–3.66 (m, 4H, 2 × $CH_2$), 3.06–2.81 (m, 8H, 4 × $CH_2$), 2.06–1.96 (m, 4H, 2 × $CH_2$), 1.62 (s, 18H, 6 × $CH_3$), 1.60 (s, 9H, 3 × $CH_3$). $^{13}$C NMR (75 MHz, $CDCl_3$) $\delta$: 164.3 (C═O), 164.1 (C═O), 164.0 (C═O), 161.3 (C═O),158.2 (C═O), 155.2 (C═O), 136.4 (CH), 136.1 (CAr), 135.4 (CAr), 135.3 (CAr), 135.0 (CAr), 133.9 (CH), 131.6 (CAr),

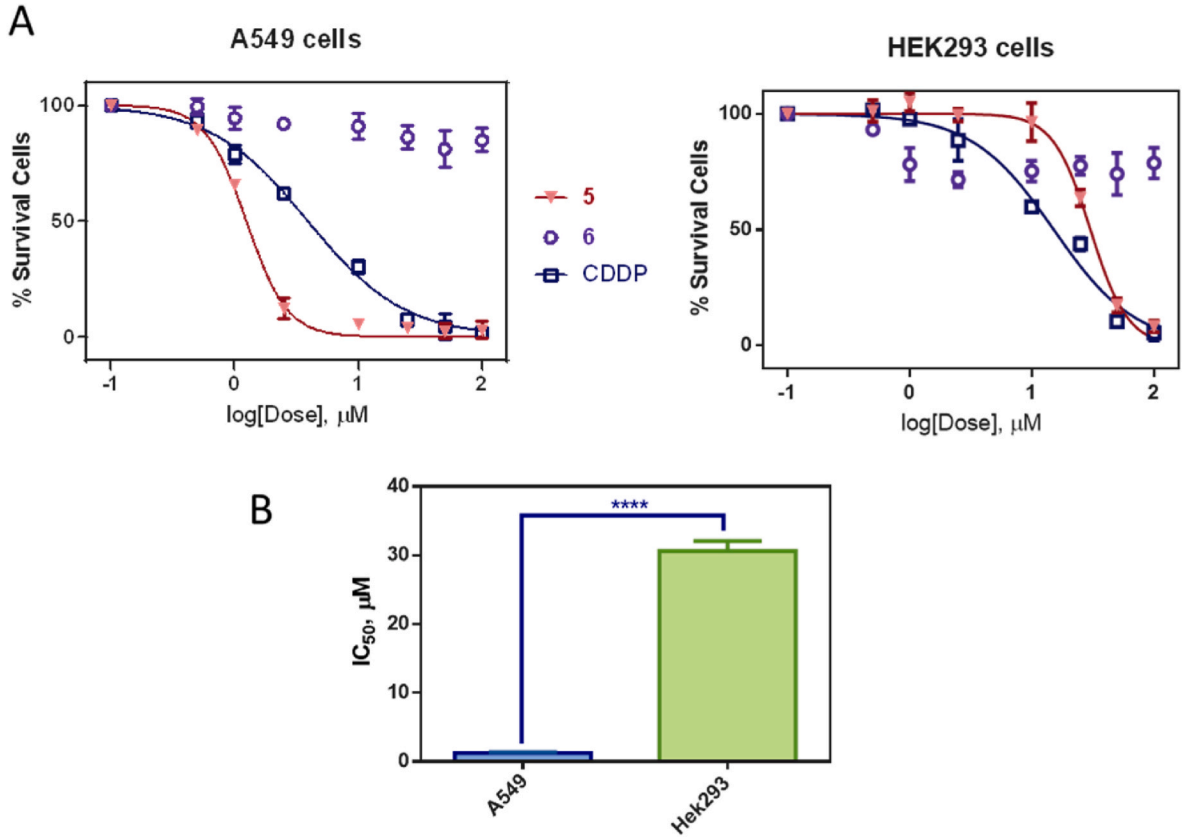


**Fig. 7.** A) Survival Curves of **5**, **6** and CDDP (positive control) in A549 and Hek293 cells after 72h of treatment. B) Half maximal inhibitory concentration ($IC_{50}$ values) of **5** in A549 and Hek293 cells. **** Statistical significance, p-value < 0.0001 (*t*-test).

131.0 (CAr), 129.7 (CAr), 125.3 (CH), 124.4 (CAr), 124.1 (CAr), 123.9 (CAr), 123.7 (CAr), 123.4 (CAr), 123.3 (CAr),121.0 (CAr), 80.8 (C), 80.2 (C), 80.2 (C), 52.7 (CH), 52.6 (CH), 44.3 ($CH_2$), 30.2 ($CH_2$), 29.1 ($CH_3$), 29.0 ($CH_3$), 28.8 ($CH_2$). HR-MS (MALDI-, DIT): *m/z* calcd. for $C_{57}H_{60}N_8O_{10}$ ($[M]^-$): 1016.4427; found: 1016.4467. UV-VIS ($CHCl_3$) $\lambda_{max}$/nm ($\varepsilon/M^{-1}\cdot cm^{-1}$): 536 (2996). Emission (Toluene, $\lambda_{ex}$ = 435 nm) $\lambda_{max}$/nm: 602. $\tau$/ns (Toluene, $\chi$2): 5.29 (57.56%) and 9.99 (42.44%) (1.10). $\Phi$ (Toluene, $\lambda_{ex}$ = 435 nm): 0.63 ± 0.01.

**General procedure for removal of *N*-Boc protecting groups.** Trifluoroacetic acid (210 μl) was added dropwise to a stirred solution of perylenediimide 3 or hemicoronene 4 (60 mg each) in $CH_2Cl_2$ (2.0 ml). The reaction mixture was stirred for 2 h. Then, aqueous NaOH (1 M) was added on the solution until basic pH (8–9). Finally, the mixture was extracted with $CH_2Cl_2$ (2 × 50 mL), the combined organic extracts were washed with water (50 mL) and dried ($MgSO_4$). Then the solvent was removed under reduced pressure to afford 5 (41 mg, 97% yield) or 6 (40 mg, 95% yield) all obtained as dark red solids.

*N*,*N*′-Bis(piperidin-1-yl)-1-((piperazin-1-yl)pyrimidin-1-yl)perylene-3,4:9,10-tetracarboxylic diimide 5. MP (°C): >350 °C. $R_f$ ($CH_2Cl_2$: MeOH, 50:4): 0.01. FT-IR (KBr, $cm^{-1}$): 3438 (N–H, amine), 2968 (C–H, aromatic), 2933 (C–H, aliphatic), 2846 (C–H, aliphatic), 1696 (C═O, imide), 1595, 1514 (C═C), 1445 (C–N), 1365 (C–N), 1330, 1201 (C–N), 1134, 832, 808, 793, 748, 720 (fingerprint region). $^1$H NMR (300 MHz, MeOD) $\delta$: 8.61–8.53 (m, 3H, 3 × Ar–H), 8.43–8.36 (m, 1H, Ar–H), 8.28–8.06 (m, 2H, 2 × Ar–H), 7.72–7.54 (m, 2H, 2 × Ar–H), 5.48–5.27 (m, 2H, 2 × N–CH), 4.22–4.18 (m, 4H, 2 × $CH_2$), 4.14–4.11 (m, 7H, 3.5 × $CH_2$), 3.63–3.57 (m, 4H, 2 × $CH_2$), 3.26–3.22 (m, 4H, 2 × $CH_2$), 3.10–3.05 (m, 4H, 2 × $CH_2$), 2.14–2.04 (m, 4H, 2 × $CH_2$). HR-MS (MALDI-, DIT): *m/z* calcd. for $C_{42}H_{38}N_8O_4$ ($[M]^-$): 718.3011; found: 718.3051. MS (MALDI+, DCTB) 5+CB [7]: *m/z* calcd. for ($C_{42}H_{38}N_8O_4$+$C_{42}H_{42}N_{28}O_{14}$) ($[M + CB [7]]^+$): 1880; found: 1879. MS (MALDI+, DCTB) 5+2CB [7]: *m/z* calcd. for ($C_{42}H_{38}N_8O_4$+2$C_{42}H_{42}N_{28}O_{14}$) ($[M+2CB [7]]^+$): 3044; found: 3048. UV-VIS ($CHCl_3$) $\lambda_{max}$/nm ($\varepsilon/M^{-1}\cdot cm^{-1}$): 530 (705). UV-VIS ($H_2O$) $\lambda_{max}$/nm ($\varepsilon/M^{-1}\cdot cm^{-1}$): 537(1708). Emission ($CHCl_3$, $\lambda_{ex}$ = 435 nm) $\lambda_{max}$/nm: 597. $\tau$/ns ($CHCl_3$ $\chi$2): 4.30 (1.28). $\Phi$ ($CHCl_3$, $\lambda_{ex}$ = 450 nm): 0.12 ± 0.01. Emission ($H_2O$, 5+CB [7], $\lambda_{ex}$ = 435 nm) $\lambda_{max}$/nm: 540. $\tau$/ns ($H_2O$, $\chi$2) 5+CB [7]: 4.59 (17.50%) and 9.54 (82.50%) (1.05). $\Phi$ ($H_2O$, $\lambda_{ex}$ = 450 nm) 5+CB [7]: 0.25 ± 0.01.

*N*,*N*′-Bis-(piperidin-4-yl)-[6,7-e]-(2-(1,4-piperazin-1-yl)-1,3-pyrimidin)perylene-3,4:9,10-tetracarboxylic diimide 6. MP (°C): >350 °C. $R_f$ ($CH_2Cl_2$:MeOH, 50:4): 0.01. FT-IR (KBr, $cm^{-1}$): 3433 (N–H, amine), 2917 (C–H, aromatic), 2855 (C–H, aliphatic), 2725 (C–H, aliphatic), 1659 (C═O, imide), 1596 (C═C), 1439 (C–N), 1370 (C–N), 1321, 1255 (C–N), 1193, 1126, 1042, 850, 795, 746, 711 (fingerprint region). $^1$H NMR (300 MHz, deuterated-TFA) $\delta$: 10.71–10.55 (m, 1H, Ar–H), 10.47–10.28 (m, 1H, Ar–H), 10.16–9.94 (m, 1H, Ar–H), 9.47–9.35 (m, 2H, 2 × Ar–H), 9.23–9.16 (m, 1H, Ar–H), 9.15–9.07 (m, 1H, Ar–H), 5.82–5.49 (m, 2H, 2 × N–CH), 4.90–4.58 (m, 4H, 2 × $CH_2$), 3.94–3.78 (m, 8H, 4 × $CH_2$), 3.47–3.25 (m, 8H, 4 × $CH_2$), 2.29–2.17 (m, 4H, 2 × $CH_2$). HR-MS (MALDI-, DIT): *m/z* calcd. for $C_{42}H_{36}N_8O_4$ ($[M]^-$): 716.2854; found: 716.2827. UV-VIS (DMSO) $\lambda_{max}$/nm ($\varepsilon/M^{-1}\cdot cm^{-1}$): 535 (10916). UV-VIS ($H_2O$) $\lambda_{max}$/nm ($\varepsilon/M^{-1}\cdot cm^{-1}$): 475 (8400). Emission (DMSO, $\lambda_{ex}$ = 430 nm) $\lambda_{max}$/nm: 646. $\tau$/ns (DMSO, $\chi$2): 1.45 (52.55%) and 4.97 (47.45%) (1.25). $\Phi$ (DMSO, $\lambda_{ex}$ = 435 nm): 0.03 ± 0.01. Emission (6+CB [7] (1:100 mol/mol in water), $\lambda_{ex}$ = 430 nm) $\lambda_{max}$/nm: 538. $\tau$/ns ($H_2O$, $\chi$2) 6+CB [7] (1:100 mol/mol in water): 4.42 (80.87%) and 10.25 (19.13%) (0.99). $\Phi$ ($H_2O$, $\lambda_{ex}$ = 435 nm) 6+CB [7] (1:100 mol/mol in water): 0.30 ± 0.01.

**Theoretical calculations.** Geometry optimizations of interaction between CB [7] and 5 or 6 have been performed with the ORCA 4.2.1 software [58,59]. For the DFT calculations, the hybrid functional B3LYP [60,61] along with double-zeta basis set def2-SVP [62] and auxiliary basis def2/J [63] for the description of all the elements. The dispersion interactions have been taken into account using the atom-pairwise dispersion correction with the Becke-Johnson damping scheme (D3BJ) [64,65]. Geometry optimizations of interaction between 5 and structure CTA22 [66] have been performed as well with the ORCA 4.2.1 software [58,59]. The structure of the telomere was downloaded from RCSB website (PDB ID: 2km3) [67] The compound 5 has been previously optimized through DFT theory using the hybrid functional B3LYP [60,61] and 6-31G** basis set for all the atoms [68]. The docking was done with the help of the AutoDock 4.0 software [69] using an efficient and durable algorithm, Lamarckian Genetic Algorithm (LGA) [70]. The conformation with the lowest binding energy was further optimized using the GFN2-xTB method [71] as it is implemented in the ORCA 4.2.1 software. The model of the complex between 5 and CTA22 was performed with PyMOL [72].

**Fluorescence enhancement experiments.** Fluorescence measurements were performed in a Shimadzu Corporation RF-5301PC spectrofluorometer (Duisburg, Germany) in a 1 cm path-length cells at 25 °C. The emission of 5 μM of the compounds under study in annealing buffer (90 mM LiCl, 10 mM lithium cacodylate (LiCaC) and 10 mM KCl at pH = 7.2) was measured in the absence and in the presence of 5 μM strand concentration of c-myc (dTGAGGGTGGGTAGGGTGGGTAA), CTA22 (dAGGGCTAGGGCTAGGGCTAGGG) and hTelo (dAGGGAGGGT AGGGTAGGGT 10 $\mu M_{BP}$ (concentration expressed in base-pairs) of ctDNA (calf thymus DNA).

**FRET Melting Assay.** FRET Melting Assay was performed in a real time Polymerase Chain Reaction (7500 Fast Real Time PCR, Applied Biosystems) as previously described [73]. Briefly, the double-labelled oligonucleotides (Table S01) were purchased from Eurogentec, were prepared in doubly deionized water at 100 μM strand concentration, and were stored at −20 °C. They have as the donor fluorophore in the 5′ end FAM (6-carboxyfluorescein) and as acceptor fluorophore TAMRA (6-carboxytetramethylrhodamine) in the 3' end oligonucleotides. For FRET working solutions, they were diluted in annealing buffer consisting of 90 mM LiCl, 10 mM LiCaC and 10 mM KCl at pH = 7.2 except for the RNA G4, 21R that it is prepared in 99 mM LiCl, 10 mM LiCaC and 1 mM KCl at pH = 7.2. Freshly solutions were prepared by heating at 90 °C during 5 min and then quickly cooled to room temperature. Then, samples containing 0.2 μM oligonucleotide in the absence and in the presence of 10 μM the complexes under study were prepared in 96-well plates and heated from 25 to 95 °C at 1 °C/min recording the emission of FAM and TAMRA. Thermal stabilization (ΔTm) was calculated as the difference between the mid-transition temperature of the oligonucleotide with and without the drug.

**Cytotoxicity.** Cytotoxicity was studied by means of the MTT Assay. For A549 Dulbecco's Modified Eagle's Medium (DMEM) was used as culture medium and for Hek293 Eagle's Minimum Essential Medium medium (EMEM) supplemented with 1% of non-essential amino acids. Both media were supplemented with 10% FBS and 1% amphotericin-penicillin-streptomycin solution. A549 and Hek293 cells were seeded in 96–well plates at a density of 3 × $10^3$ and 1 × $10^4$ cells/well and incubated at 37 °C under a 5% $CO_2$ atmosphere. Cells were treated with different concentrations of the compounds under study during 72 h. Then, treatment was removed and cells were incubated with 100 μl of MTT (3-(4,5-dimethyltiazol-2-yl)-2,5-diphenyltetrazolium bromide) (Sigma Aldrich) dissolved in culture medium (500 μg/ml). After 4h, 100 μl of solubilizing solution (10% (w/v) SDS, 0.01 M HCl) were added to each well and incubated for other 18 h. At the end, absorbance at 590 nm was read in a microplate reader (Cytation 5 Cell Imaging Multi-Mode Reader - Biotek Instruments, USA). Four replicates per dose were included. The $IC_{50}$ values were calculated from cell survival data of at least two independent experiments using GraphPadPrism Software Inc. version 6.01 (USA). In every case, cell death was confirmed by microscopy visualization of the treated cells.

**Bioimaging experiments.** A549 and HEK293 cells were seeded in appropriated 96-well plates at a density of 3 × $10^3$ cells/well in 200 μL DMEM at pH = 7.4 without phenol red and allow to adhere for 24 h at 37 °C and 5% $CO_2$. Then, cells were treated with different concentrations of compounds under study and incubated at 37 °C under 5% $CO_2$

atmosphere for 4 h. Finally, cells were visualized in a Cytation 5 Cell Imaging Multi-Mode Reader (Biotek Instruments, USA) in bright field and orange fluorescence emission with a 20 × objective.

## 4. Conclusions

In conclusion, we have prepared a new series of perylene and hemicoronene diimides. Among them, four compounds were obtained upon irradiation with visible light that leads to the photocyclization products. The perylene **5** and its hemicoronene analogue **6** were remarkable examples of water soluble compounds able to form nanoparticles by self-association. These compounds that are not fluorescent in their self-associated form become fluorescent materials due to their disassociation caused by complexation with cucurbit[7]uril. Both compounds were selective G-quadruplex binding ligands, being the perylenediimide **5** the most sensitive compound since its emission was highly enhanced in the presence of G4 structures. In addition, only **5** was a cytotoxic compound, being more active against A549 lung adenocarcinoma cells than against the non-cancer Hek293 cells. That is, in terms of cytotoxicity, we could conclude that for this compound photocyclization is synonymous of inactivation.

## Author contributions

D. C. R, A. R.-C. and T. R. performed the synthesis and characterization of all compounds. D. C. R, and I. R. performed the titration experiments. N. B. and B. G. designed and performed the experiments of G-quadruplex binding and cytotoxicity; J. V. C. performed the theoretical calculations. T. T. designed the synthesis and titration experiments and, in collaboration with N. B. and J. V. C., wrote the manuscript. All authors read and approved the manuscript.

## Declaration of competing interest

The authors declare that they have no known competing financial interests or personal relationships that could have appeared to influence the work reported in this paper.

## Data availability

Data will be made available on request.

## Acknowledgements

We acknowledge the Ministerio de Ciencia, Innovación y Universidades-FEDER (Grants PID2019-111215RB-100 and RTI2018-102040-B-100), the Junta de Castilla y León, Consejería de Educación y Cultura y Fondo Social Europeo (Grants BU263P18 and BU305P18), "la Caixa" Foundation (LCF/PR/PR12/11070003) for financial support. A. R.C. thanks Secretaría General de Universidades for a FPU18/03225 Grant. This research has made use of the high-performance computing resources of the Castilla y León Supercomputing Center (SCAYLE, https://www.scayle.es), financed by FEDER (Fondo Europeo de Desarrollo Regional). We thank Ms. M[a] del Pilar Castroviejo-Fernández, from PCT, UBU, for assistance in AFM studies and Mr. Javier Gutierrez-Reguera from LTI, UVA, for assistance in DLS studies.

## Appendix A. Supplementary data

Supplementary data to this article can be found online at https://doi.org/10.1016/j.dyepig.2022.110557.

## References

[1] Wani WA, Shahid M, Hussain A, AlAjmi MF. Fluorescent organic nanoparticles, new generation materials with diverse analytical and biomedical applications. Singapore: Springer Briefs in Materials, Springer Nature; 2018. https://doi.org/10.1007/978-981-13-2655-4.
[2] Rwei AY, Wang W, Kohane DS. Photoresponsive nanoparticles for drug delivery. Nano Today 2015;10:451–67. https://doi.org/10.1016/j.nantod.2015.06.004.
[3] Reisch A, Klymchenko AS. Fluorescent polymer nanoparticles based on dyes: seeking brighter tools for bioimaging. Small 2016;12:1968–92. https://doi.org/10.1002/smll.201503396.
[4] Chan YH, Wu PJ. Semiconducting polymer nanoparticles as fluorescent probes for biological imaging and sensing. Part Part Syst Char 2015;32:11–28. https://doi.org/10.1002/ppsc.201400123.
[5] Gao M, Tang BZ. Fluorescent sensors based on aggregation-induced emission: recent advances and perspectives. ACS Sens 2017;2:1382–99. https://doi.org/10.1021/acssensors.7b00551.
[6] Tang Y, Tang BZ, editors. Principles and applications of aggregation-induced emission. Switzerland: Springer Nature; 2019. https://doi.org/10.1007/978-3-319-99037-8.
[7] Würthner F. Perylene bisimide dyes as versatile building blocks for functional supramolecular architectures. Chem Commun 2004:1564–79. https://doi.org/10.1039/B401630K.
[8] Chen Z, Lohr A, Saha-Möller CR, Würthner F. Self-assembled p-stacks of functional dyes in solution: structural and thermodynamic features. Chem Soc Rev 2009;38:564–84. https://doi.org/10.1039/B809359H.
[9] Würthner F, Kaiser TE, Saha-Möller CR. J-aggregates: from serendipitous discovery to supramolecular engineering of functional dye materials. Angew Chem Int Ed 2011;50:3376–410. https://doi.org/10.1002/anie.201002307.
[10] Safont-Sempere MM, Fernández G, Würthner F. Self-sorting phenomena in complex supramolecular systems. Chem Rev 2011;111:5784–814. https://doi.org/10.1021/cr100357h.
[11] Würthner F, Saha-Möller CR, Fimmel B, Ogi S, Leowanawat P, Schmidt D. Perylene bisimide dye assemblies as archetype functional supramolecular materials. Chem Rev 2016;116:962–1052. https://doi.org/10.1021/acs.chemrev.5b00188.
[12] Görl D, Zhang X, Stepanenko V, Würthner F. Supramolecular block copolymers by kinetically controlled co-self-assembly of planar and core-twisted perylene bisimides. Nat Commun 2015;6:7009. https://doi.org/10.1038/ncomms8009.
[13] Su F, Chen G, Korevaar PA, Pan F, Liu H, Guo Z, Schenning APHJ, Zhang HJ, Lin J, Jiang YB. Discrete p-stacks from self-assembled perylenediimide analogues. Angew Chem Int Ed 2019;58:15273–7. https://doi.org/10.1002/anie.201907838.
[14] Görl D, Zhang X, Würthner F. Molecular assemblies of perylene bisimide dyes in water. Angew Chem Int Ed 2012;51:6328–48. https://doi.org/10.1002/anie.201108690.
[15] Schill J, Schenning APHJ, Brunsveld L. Self-Assembled fluorescent nanoparticles from π-conjugated small molecules: en route to biological applications, macromol. Rapid Commun 2015;36:1306–21. https://doi.org/10.1002/marc.201500117.
[16] Yang SK, Shi X, Park S, Doganay S, Ha T, Zimmerman SC. Monovalent, Clickable, Uncharged, Water-soluble perylenediimide-cored dendrimers for target-specific fluorescent biolabeling. J Am Chem Soc 2011;133:9964–7. https://doi.org/10.1021/ja2009136.
[17] Ji C, Cheng W, Yuan Q, Müllen K, Yin M. From dyestuff chemistry to cancer theranostics: the rise of rylenecarboximides. Acc Chem Res 2019;52:2266–77. https://doi.org/10.1021/acs.accounts.9b00221.
[18] Lü B, Chen Y, Li P, Wang B, Müllen K, Yin M. Stable radical anions generated from a porous perylenediimide metal-organic framework for boosting near-infrared photothermal conversion. Nat Commun 2019;10:767. https://doi.org/10.1038/s41467-019-08434-4.
[19] Liu C, Zhang S, Li J, Wei J, Müllen K, Yin M. A water-soluble, NIR-absorbing quaterrylenediimide chromophore for photoacoustic imaging and efficient photothermal cancer therapy. Angew Chem Int Ed 2019;58:1638–42. https://doi.org/10.1002/anie.201810541.
[20] Yang Z, Chen X. Semiconducting perylene diimide nanostructure: multifunctional phototheranostic nanoplatform. Acc Chem Res 2019;52:1245–54. https://doi.org/10.1021/acs.accounts.9b00064.
[21] Nagarajan K, Mallia AR, Muraleedharan K, Hariharan M. Enhanced intersystem crossing in core-twisted aromatics. Chem Sci 2017;8:1776–82. https://doi.org/10.1039/C6SC05126J.
[22] Schuster NJ, Paley DW, Jockusch S, Ng F, Steigerwald ML, Nuckolls C. Electron delocalization in perylene diimide helicenes. Angew Chem Int Ed 2016;55:13519–23. https://doi.org/10.1002/anie.201607878.
[23] Fu H, Meng D, Meng X, Sun X, Huo L, Fan Y, Li Y, Ma W, Sun Y, Wang Z. Influence of alkyl chains on photovoltaic properties of 3D rylene propeller electron acceptors. J Mater Chem 2017;5:3475–82. https://doi.org/10.1039/C6TA09049D.
[24] Cai Z, Vázquez RJ, Zhao D, Li L, Lo WY, Zhang N, Wu Q, Keller B, Eshun A, Abeyasinghe N, Banaszak-Holl H, Goodson III T, Yu L. Two photon absorption study of low-bandgap, fully conjugated perylene diimide-thienoacene-perylene diimide ladder-type molecules. Chem Mater 2017;29:6726–32. https://doi.org/10.1021/acs.chemmater.7b01512.
[25] Ziffer ME, Jo SB, Zhong H, Ye L, Liu H, Lin F, Zhang J, Li X, Ade HW, Jen AKY, Ginger DS. Long-lived, non-geminate, radiative recombination of photogenerated charges in a polymer/small-molecule acceptor photovoltaic blend. J Am Chem Soc 2018;140:9996–10008. https://doi.org/10.1021/jacs.8b05834.
[26] Wu M, Yi JP, Chen L, He G, Chen F, Sfeir MY, Xia J. Novel star-shaped helical perylene diimide electron acceptors for efficient additive-free nonfullerene organic solar cells. ACS Appl Mater Interfaces 2018;10:27894–901. https://doi.org/10.1021/acsami.8b06126.
[27] Milton M, Schuster NJ, Paley DW, Sánchez RH, Ng F, Steigerwald ML, Nuckolls C. Defying strain in the synthesis of an electroactive bilayer helicene. Chem Sci 2019;10:1029–34. https://doi.org/10.1039/C8SC04216K.

[28] Busto N, Calvo P, Santolaya J, Leal JM, Guédin A, Barone G, Torroba T, Mergny JL, García B. Fishing for G-Quadruplexes in solution with a perylene diimide derivative labeled with biotins. Chem Eur J 2018;24:11292–6. https://doi.org/10.1002/chem.201802365.

[29] Micheli E, Altieri A, Cianni L, Cingolani C, Iachettini S, Bianco A, Leonetti C, Cacchione S, Biroccio A, Franceschin M, Rizzo A. Perylene and coronene derivatives binding to G-rich promoter oncogene sequences efficiently reduce their expression in cancer cells. Biochimie 2016;125:223–31. https://doi.org/10.1016/j.biochi.2016.04.008.

[30] Franceschin M, Rizzo A, Casagrande V, Salvati E, Alvino A, Altieri A, Ciammaichella A, Iachettini S, Leonetti C, Ortaggi G, Porru M, Bianco A, Biroccio A. Aromatic core extension in the series of N-cyclic bay-substituted perylene G-quadruplex ligands: increased telomere damage, antitumor activity, and strong selectivity for neoplastic over healthy cells. ChemMedChem 2012;7:2144–54. https://doi.org/10.1002/cmdc.201200348.

[31] Franceschin M, Alvino A, Casagrande V, Mauriello C, Pascucci E, Savino M, Ortaggi G, Bianco A. Specific interactions with intra- and intermolecular G-quadruplex DNA structures by hydrosoluble coronene derivatives: a new class of telomerase inhibitors. Bioorg Med Chem 2007;15:1848–58. https://doi.org/10.1016/j.bmc.2006.11.032.

[32] Porru M, Zizza P, Franceschin M, Leonetti C, Biroccio A, EMICORON. A multi-targeting G4 ligand with a promising preclinical profile. Biochim Biophys Acta 2017;1861:1362–70. https://doi.org/10.1016/j.bbagen.2016.11.010.

[33] Bhasikuttan AC, Mohanty J. Targeting G-quadruplex structures with extrinsic fluorogenic dyes: promising fluorescence sensors. Chem Commun 2015;51:7581–97. https://doi.org/10.1039/C4CC10030A.

[34] Ma DL, Zhang Z, Wang M, Lu L, Zhong HJ, Leung CH. Recent developments in G-quadruplex probes. Chem Biol 2015;22:812–28. https://doi.org/10.1016/j.chembiol.2015.06.016.

[35] Sengupta A, Roy SS, Chowdhury S. Non-duplex G-quadruplex DNA structure: a developing story from predicted sequences to DNA structure-dependent epigenetics and beyond. Acc Chem Res 2021;54:46–56. https://doi.org/10.1021/acs.accounts.0c00431.

[36] Liu LY, Liu W, Wang KN, Zhu BC, Xia XY, Ji LN, Mao ZW. Quantitative detection of G-quadruplex DNA in live cells based on photon counts and complex structure discrimination. Angew Chem Int Ed 2020;59:9719–26. https://doi.org/10.1002/anie.202002422.

[37] Zhang S, Sun H, Wang L, Liu Y, Chen H, Li Q, Guan A, Liu M, Tang Y. Real-time monitoring of DNA G-quadruplexes in living cells with a small-molecule fluorescent probe. Nucleic Acids Res 2018;46:7522–32. https://doi.org/10.1093/nar/gky665.

[38] García-Calvo J, Robson JA, Torroba T, Wilton-Ely JDET. Synthesis and application of ruthenium(II) alkenyl complexes with perylene fluorophores for the detection of toxic vapours and gases. Chem Eur J 2019;25:14214–22. https://doi.org/10.1002/chem.201903303.

[39] García-Calvo J, Calvo-Gredilla P, Ibáñez-Llorente M, Romero DC, Cuevas JV, García-Herbosa G, Avella M, Torroba T. Surface functionalized silica nanoparticles for the off–on fluorogenic detection of an improvised explosive, TATP, in a vapour flow. J Mater Chem 2018;6:4416–23. https://doi.org/10.1039/C7TA10792G.

[40] Romero DC, Calvo-Gredilla P, García-Calvo J, Diez-Varga A, Cuevas JV, Revilla-Cuesta A, Busto N, Abajo I, Aullón G, Torroba T. Self-assembly hydrosoluble coronenes: a rich source of supramolecular turn-on fluorogenic sensing materials in aqueous media. Org Lett 2021;23. https://doi.org/10.1021/acs.orglett.1c03175. 8727−8732.

[41] Pazos E, Novo P, Peinador C, Kaifer AE, García MD. Cucurbit[8]uril (CB[8])-Based supramolecular switches. Angew Chem Int Ed 2019;58:403–16. https://doi.org/10.1002/anie.201806575.

[42] Liu J, Lan Y, Yu Z, Tan CSY, Parker RM, Abell C, Scherman OA. Cucurbit[n]uril-Based microcapsules self-assembled within microfluidic droplets: a versatile approach for supramolecular architectures and materials. Acc Chem Res 2017;50:208–17. https://doi.org/10.1021/acs.accounts.6b00429.

[43] Mako TL, Racicot JM, Levine M. Supramolecular luminescent sensors. Chem Rev 2019;119. https://doi.org/10.1021/acs.chemrev.8b00260. 322−477.

[44] Kim HJ, Nandajan PC, Gierschner J, Park SY. Light-harvesting fluorescent supramolecular block copolymers based on cyanostilbene derivatives and cucurbit[8]urils in aqueous solution. Adv Funct Mater 2017;1705141. https://doi.org/10.1002/adfm.201705141.

[45] Biedermann F, Elmalem E, Ghosh I, Nau WM, Scherman OA. Strongly fluorescent, switchable perylene bis(diimide) host–guest complexes with cucurbit[8]uril in water. Angew Chem Int Ed 2012;51:7739–43. https://doi.org/10.1002/anie.201202385.

[46] Liu K, Yao Y, Kang Y, Liu Y, Han Y, Wang Y, Li Z, Zhang X. A supramolecular approach to fabricate highly emissive smart materials. Sci Rep 2013;3:2372. https://doi.org/10.1038/srep02372.

[47] Thomas SS, Tang H, Bohne C. Noninnocent role of Na+ ions in the binding of the N-Phenyl-2-naphthylammonium cation as a ditopic guest with cucurbit[7]uril. J Am Chem Soc 2019;141:9645–54. https://doi.org/10.1021/jacs.9b03691.

[48] Yang X, Wang R, Kermagoret A, Bardelang D. Oligomeric cucurbituril complexes: from peculiar assemblies to emerging applications. Angew Chem Int Ed 2020;59:21280–92. https://doi.org/10.1002/anie.202004622.

[49] Wu G, Bae YJ, Olesinska M, Antón-García D, Szabó I, Rosta E, Wasielewski MR, Scherman OA. Controlling the structure and photophysics of fluorophore dimers using multiple cucurbit[8]uril clampings. Chem Sci 2020;11:812–25. https://doi.org/10.1039/C9SC04587B.

[50] Thompson NA, Barbero H, Masson E. Templating conformations with cucurbiturils. Chem Commun 2019;55:12160–3. https://doi.org/10.1039/C9CC06766C.

[51] Palma A, Artelsmair M, Wu G, Lu X, Barrow SJ, Uddin N, Rosta E, Masson E, Scherman OA. Cucurbit[7]uril as a supramolecular artificial enzyme for diels–alder reactions. Angew Chem Int Ed 2017;56:15688–92. https://doi.org/10.1002/anie.201706487.

[52] Guagnini F, Antonik PM, Rennie ML, O'Byrne P, Khan AR, Pinalli R, Dalcanale E, Crowley PB. Cucurbit[7]uril-Dimethyllysine recognition in a model protein. Angew Chem Int Ed 2018;57:7126–30. https://doi.org/10.1002/anie.201803232.

[53] Schoder S, Schröder HV, Cera L, Puttreddy R, Gettler A, Resch-Genger U, Rissanen K, Schalley CA. Strong emission enhancement in pH-responsive 2:2 cucurbit[8]uril complexes. Chem Eur J 2019;25:3257–61. https://doi.org/10.1002/chem.201806337.

[54] Maity D, Assaf KI, Sicking W, Hirschhäuser C, Nau WM, Schmuck C. A selective cucurbit[8]uril-peptide beacon ensemble for the ratiometric fluorescence detection of peptides. Chem Eur J 2019;25:13088–93. https://doi.org/10.1002/chem.201901037.

[55] http://supramolecular.org/. [Accessed 26 January 2021].

[56] Thordarson P. Determining association constants from titration experiments in supramolecular chemistry. Chem Soc Rev 2011;40:1305–23. https://doi.org/10.1039/C0CS00062K.

[57] Hibbert DB, Thordarson P. The death of the Job plot, transparency, open science and online tools, uncertainty estimation methods and other developments in supramolecular chemistry data analysis. Chem Commun 2016;52:12792–805. https://doi.org/10.1039/C6CC03888C.

[58] Neese F, The ORCA Program System. WIREs Comput Mol Sci 2012;2:73–8.

[59] Neese F. Software update: the ORCA program system, version 4.0. WIREs Comput Mol Sci 2018;8:e1327. https://doi.org/10.1002/wcms.81.

[60] Becke AD. Density-functional thermochemistry. III. The role of exact exchange. J Chem Phys 1993;98:5648–52. https://doi.org/10.1063/1.464913.

[61] Lee CT, Yang WT, Parr RG. Development of the Colle-Salvetti correlation-energy formula into a functional of the electron density. Phys Rev B 1988;37:785–9. https://doi.org/10.1103/PhysRevB.37.785.

[62] Weigend F, Ahlrichs R. Balanced basis sets of split valence, triple zeta valence and quadruple zeta valence quality for H to Rn: design and assessment of accuracy. Phys Chem Chem Phys 2005;7:3297–305. https://doi.org/10.1039/B508541A.

[63] Weigend F. Accurate coulomb-fitting basis sets for H to Rn. Phys Chem Chem Phys 2006;8:1057–65. https://doi.org/10.1039/B515623H.

[64] Grimme S, Antony J, Ehrlich S, Krieg H. A consistent and accurate ab initio parametrization of density functional dispersion correction (DFT-D) for the 94 elements H-Pu. J Chem Phys 2010;132:154104. https://doi.org/10.1063/1.3382344.

[65] Grimme S, Ehrlich S, Goerigk L. Effect of the damping function in dispersion corrected density functional theory. J Comput Chem 2011;32:1456–65. https://doi.org/10.1002/jcc.21759.

[66] Lim KW, Alberti P, Guédin A, Lacroix L, Riou JF, Royle NJ, Mergny JL, Phan AT. Sequence variant (CTAGGG)n in the human telomere favors a G-quadruplex structure containing a G·C·G·C tetrad. Nucleic Acids Res 2009;37:6239–48. https://doi.org/10.1093/nar/gkp630.

[67] https://www.rcsb.org/structure/2KM3. [Accessed 26 November 2021].

[68] Hariharan PC, Pople JA. The influence of polarization functions on molecular orbital hydrogenation energies. Theor Chim Acta 1973;28:213–22. https://doi.org/10.1007/BF00533485.

[69] Morris GM, Huey R, Lindstrom W, Sanner MF, Belew RK, Goodsell DS, Olson AJ. AutoDock4 and AutoDockTools4: automated docking with selective receptor flexibility. J Comput Chem 2009;30:2785–91. https://doi.org/10.1002/jcc.21256.

[70] Morris GM, Goodsell DS, Halliday RS, Huey R, Hart WE, Belew RK, Olson AJ. Automated docking using a Lamarckian genetic algorithm and an empirical binding free energy function. J Comput Chem 1998;19:1639–62. https://doi.org/10.1002/(SICI)1096-987X(19981115)19:14<1639::AID-JCC10>3.0.CO;2-B.

[71] Bannwarth C, Ehlert S, Grimme S. GFN2-xTB—an accurate and broadly parametrized self-consistent tight-binding quantum chemical method with multipole electrostatics and density-dependent dispersion contributions. J Chem Theor Comput 2019;15:1652–71. https://doi.org/10.1021/acs.jctc.8b01176.

[72] The PyMOL molecular graphics system, version 2.0 Schrödinger, LLC.

[73] De Rache A, Mergny JL. Assessment of selectivity of G-quadruplex ligands via an optimised FRET melting assay. Biochimie 2015;115:194–202. https://doi.org/10.1016/j.biochi.2015.06.002.